

PREDICTIVE MODELING OF MIXED HALIDE PEROVSKITE CELL USING HYBRID L_{27} OA TAGUCHI-BASED GA-MLR-GA APPROACH

Khairil Ezwan Kaharudin, Fauziyah Salehuddin

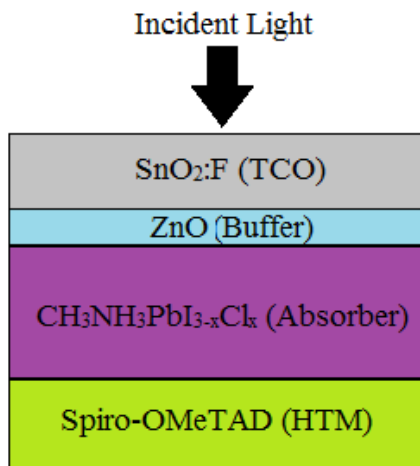
Faculty of Electronics and Computer Engineering (FKEKK), Universiti Teknikal Malaysia Melaka (UTeM), Hang Tuah Jaya, 76100 Durian Tunggal, Melaka, Malaysia

Article history

Received
9 August 2020
Received in revised form
28 October 2021
Accepted
7 October 2021
Published Online
20 December 2021

*Corresponding author
fauziyah@utem.edu.my

Graphical abstract



Abstract

Perovskite photovoltaic cell is regarded as an alternative configuration for the conventional photovoltaic cells predominantly due to its high efficiency. In this paper, a predictive modeling using a hybrid L_{27} orthogonal array (OA) Taguchi-based Grey relational analysis (GRA), multiple linear regression (MLR) and genetic algorithm (GA) was proposed to optimize the device parameters for better overall performance. The Perovskite photovoltaic cell model is initially constructed and simulated using solar cell capacitance simulator (SCAPS). The final results reveal that the proposed hybrid L_{27} OA Taguchi-based GRA-MLR-GA approach has effectively optimized the device parameters in which SnO₂:F thickness, SnO₂:F donor density, ZnO thickness, ZnO donor density, CH₃NH₃PbI_{3-x}Cl_x thickness, CH₃NH₃PbI_{3-x}Cl_x donor density, Spiro-OMeTAD thickness and Spiro-OMeTAD acceptor density are predictively tuned at 0.198 μm , 8.973 $\times 10^{18}$ cm^{-3} , 0.039 μm , 8.827 $\times 10^{17}$ cm^{-3} , 0.386 μm , 1.929 $\times 10^{13}$ cm^{-3} , 0.233 μm and 8.984 $\times 10^{18}$ cm^{-3} respectively. After the predictive modeling, both FF and PCE of the perovskite photovoltaic cell have been improved for ~5.93% and ~5.78% respectively.

Keywords: FF, genetic algorithm, PCE, Photovoltaic, Taguchi based GRA

Abstrak

Sel fotovoltaik perovskite ialah suatu konfigurasi alternatif kepada sel fotovoltaik konvensional kerana mempunyai kecekapan yang tinggi. Dalam kertas kerja ini, pemodelan prediktif menggunakan kaedah gabungan L_{27} tatasusunan ortogonal (OA) Taguchi berasaskan analisis perhubungan Grey (GRA), regresi linear berganda (MLR) dan algoritma genetik (GA) telah dicadangkan bagi mengoptimumkan parameter peranti dalam mencapai prestasi yang lebih baik. Model peranti mulanya dibina dan disimulasikan menggunakan simulator SCAPS. Hasil akhir menunjukkan bahawa pendekatan GRA-MLR-GA berasaskan L_{27} OA Taguchi hibrid yang dicadangkan telah mengoptimumkan parameter peranti dengan berkesan di mana ketebalan SnO₂:F, ketumpatan penderma SnO₂:F, ketebalan ZnO, ketumpatan penderma ZnO, ketebalan CH₃NH₃PbI_{3-x}Cl_x, ketumpatan penderma CH₃NH₃PbI_{3-x}Cl_x, ketebalan Spiro-OMeTAD dan ketumpatan penerima Spiro-OMeTAD telah dilaraskan secara prediktif kepada 0.198 μm , 8.973 $\times 10^{18}$ cm^{-3} , 0.039 μm , 8.827 $\times 10^{17}$ cm^{-3} , 0.386 μm , 1.929 $\times 10^{13}$ cm^{-3} , 0.233 μm and 8.984 $\times 10^{18}$ cm^{-3} . Selepas pemodelan prediktif, FF and PCE sel fotovoltaik perovskite telah dipertingkatkan sebanyak ~5.93% and ~5.78%.

Kata kunci: Algoritma genetik, FF, PCE, Fotovoltaik, Taguchi berasaskan GRA

© 2022 Penerbit UTM Press. All rights reserved

1.0 INTRODUCTION

In the past years, numerous researches in mixed-halide Perovskite photovoltaic cells have been actively conducted predominantly due to their process ability, reduced-weight and remarkable power conversion efficiency which are very crucial for low-cost thin-film photovoltaic industry. The mixed-halide Perovskite technology offers the ease of fabrication process with low cost and energy payback time suitable for substituting current silicon-based photovoltaic cells. The initial reported photovoltaic cell utilizing Perovskite ($\text{CH}_3\text{NH}_3\text{PbI}_3$) gained power conversion efficiency (PCE) of 3.81% back in year 2009 [1] which then tremendously increased beyond 20% in recent days [2, 3, 4].

The most important attribute of the mixed-halide Perovskite device is the fine-tuned energy band gap absorber layer which can be performed by tuning mixed-halide elements before undergoing photo activation. The most prevalent mixed-halide Perovskites used in photovoltaic cell are $\text{CH}_3\text{NH}_3\text{PbI}_{3-x}\text{Cl}_x$ and $\text{CH}_3\text{NH}_3\text{PbI}_{3-x}\text{Br}_x$ which offers numerous advantages such as lesser carrier recombination, improved device stability, enhanced carrier transport, increased carrier diffusion length and wideband optical absorptions [5, 6].

For Perovskite-based structure, the absorber layer of $\text{CH}_3\text{NH}_3\text{PbI}_{3-x}\text{Cl}_x$ is commonly stacked adjacent to electron material transport (ETM) and hole material transport (HTM). Most of the majority carriers either electrons or holes are generated after the event of light absorption in which the incident photon excites the electrons/holes propagate through the conducting path. This signifies the importance of carrier pathway from absorber to both cathode and anode, creating an enormous impact on Perovskite-based devices [7, 8, 9]. Despite the continuous improvement of Perovskite photovoltaic cells, it is still necessary to further comprehend the interrelationship between the layer parameters and the output performances. Numerical simulation is one of the effective ways to conduct extensive investigation on each layer parameters of the Perovskite devices [10, 11, 12].

In addition, the numerical simulation could be combined with numerous statistical and machine learning approaches in identifying the optimal solution for better output performances [13, 14, 15]. The main advantage of these approaches is to provide predictive insight on the device performances before undergoing actual experimental and fabrication process which definitely saving a lot of time and cost [16, 17, 18]. This work will focus on the optimization of the mixed-halide Perovskite photovoltaic cell using numerical simulation with the aid of a hybrid L_{27} orthogonal array (OA) Taguchi-based grey relational analysis (GRA), multiple linear regression (MLR) and genetic algorithm (GA). This approach is preferred over common optimization methods (response surface methodology (RSM), Taguchi method and etc.) primarily due to taking advantage on genetic

algorithm which use objective function information, not derivatives. Furthermore, the utilization of grey relational analysis eases the computation process especially when it involves many responses and parameters that need to be analyzed simultaneously.

2.0 METHODOLOGY

The methodology of this current work consists of two primary stages which are device simulation and predictive modeling. The device simulation of the Perovskite photovoltaic cell is initially carried out using solar cell capacitance simulator (SCAPS) which is a well-known open source one-dimensional software developed by the Department of Electronics and Information Systems (ELIS) of the University of Gent, Belgium [19]. Predictive modeling is later conducted to further optimize multiple device parameters upon achieving much better *FF* and *PCE*. The detail information for both device simulation and predictive modeling will be explained in the following sub-chapters.

2.1 Device Simulation

The simulation of Perovskite photovoltaic cell was performed using SCAPS (version 3.3.02) where its numerical computation is based on the fundamental semiconductor equations such as hole continuity, electron continuity and Poisson equations as can be mathematically described in (1), (2) and (3) respectively:

$$\frac{dp_n}{dt} = G_p - \frac{p_n - p_{n0}}{\tau_p} - p_n \mu_p \frac{d\xi}{dx} - \mu_p \xi \frac{dp_n}{dx} + D_p \frac{d^2 p_n}{dx^2} \quad (1)$$

$$\frac{dn_p}{dt} = G_n - \frac{n_p - n_{p0}}{\tau_n} + n_p \mu_n \frac{d\xi}{dx} + \mu_p \xi \frac{dn_p}{dx} + D_p \frac{d^2 n_p}{dx^2} \quad (2)$$

$$\frac{d}{dx} \left(-\varepsilon(x) \frac{d\psi}{dx} \right) = q [p(x) - n(x) + N_a^+(x) - N_d^-(x) + p_t(x) - n_t(x)] \quad (3)$$

for which $N_a^-(x)$ and $N_d^+(x)$ represent the ionized acceptor and donor doping density respectively, $p(x)$, $n(x)$, $p_t(x)$ and $n_t(x)$ denote free holes, free electrons, trapped holes and trapped electrons accordingly, G represents rate of generation, q represents electron charges, D represents diffusion coefficients, x represents the direction across device thickness, ψ represents electrostatic potential and ξ represents electric field. The recombination and current density-voltage characteristic together with the magnitude of open circuit voltage (V_{oc}), short circuit current density (J_{sc}), fill factor (*FF*) and power conversion efficiency (*PCE*) can be extracted by solving the aforementioned equations.

The cell configuration constructed in this simulation is depicted in Figure 1 in which spray pyrolyzed fluorine-doped tin oxide ($\text{SnO}_2:\text{F}$) and zinc oxide (ZnO)

were utilized as n-type transparent conducting oxide (TCO) and buffer layers respectively. Additionally, the metal work function for the front contact and back contact of the device were set at 4.4 eV and 5.1 eV respectively. Mixed Halide Perovskite ($\text{CH}_3\text{NH}_3\text{PbI}_{3-x}\text{Cl}_x$) was employed as the absorber layer to lightly harvest efficient electrons and holes transportation. Moreover, the Spiro-OMeTAD was used as hole transport material (HTM) mainly due to its efficient charge extraction and stability in photovoltaic cell configuration.

Device parameters employed in this numerical simulation including the layer thickness and doping density are referred to previous works [7, 20, 21] as summarized in Table 1. The term χ , ϵ_r , E_g , μ_n , μ_p , N_v , N_c , N_a , N_d and N_t in Table 1 stand for electron affinity, relative permittivity, bandgap energy, electron mobility, hole mobility, effective valence band density, effective conduction band density, acceptor density, donor density and defect density respectively. In this simulation, the effect of shunt and series resistance was not considered because it is typically caused by manufacturing defects, rather than poor photovoltaic design. The defects include the resistances of the top and rear metal contacts, as well as the contact resistance between the metal contact and the body. The defect density (N_t) of every layer except absorber layer were equally set at 10^{15} cm^{-3} . For the absorber layer ($\text{CH}_3\text{NH}_3\text{PbI}_{3-x}\text{Cl}_x$), the magnitude of N_t was set at $2.5 \times 10^{13} \text{ cm}^{-3}$. The simulations were constantly conducted under the standard AM 1.5 spectrum at 300 K of temperature.

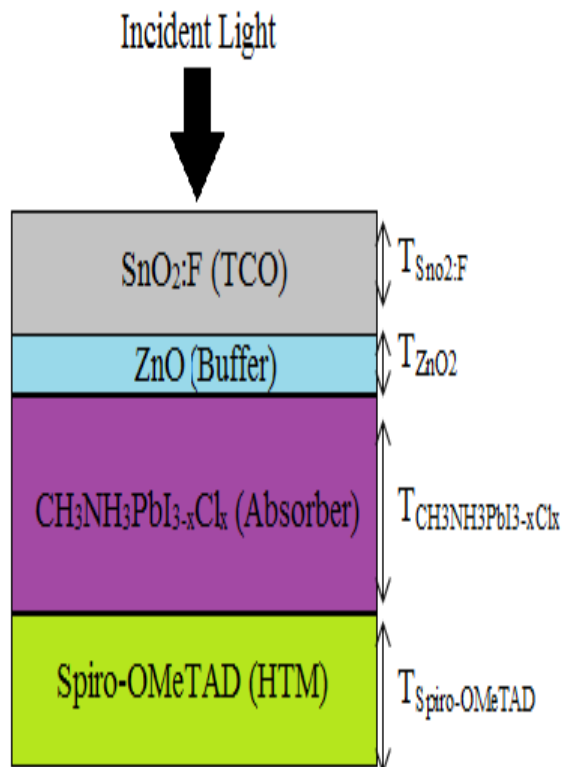


Figure 1 Cross-sectional structure of Perovskite photovoltaic cell

Table 1 Baseline Parameters for Perovskite Photovoltaic Cell

Parameters	SnO ₂ :F (TCO)	ZnO (Buffer)	CH ₃ NH ₃ PbI _{3-x} Cl _x (Absorber)	Spiro-OMeTAD (HTM)
Thickness (μm)	0.2	0.04	0.4	0.25
χ (eV)	4	3.9	3.9	2.45
ϵ_r	9	9	6.5	3
E_g (eV)	3.5	3.3	1.55	3.0
μ_n (cm ² /Vs)	20	50	2	2×10^{-4}
μ_p (cm ² /Vs)	10	5	2	2×10^{-4}
N_v (cm ⁻³)	1.8×10^{19}	1×10^{19}	1.8×10^{19}	1.8×10^{19}
N_c (cm ⁻³)	2.2×10^{18}	1×10^{19}	2.2×10^{18}	2.2×10^{18}
N_a (cm ⁻³)	-	-	-	2×10^{18}
N_d (cm ⁻³)	1×10^{18}	5×10^{17}	10^{13}	-
N_t (cm ⁻³)	10^{15}	10^{15}	2.5×10^{13}	10^{15}

2.1 Predictive Modeling

In this section, a description of the proposed predictive modeling approach used for optimizing the Perovskite photovoltaic cell will be discussed in detail. In this simulation work, the device was predictively modeled via a combination of L_{27} orthogonal array (OA) Taguchi-based Grey relational analysis-multiple linear regression-genetic algorithm (GRA-MLR-GA) approach. Figure 2 depicts the overall flowchart of the predictive modeling using L_{27} OA Taguchi-based GRA-MLR-GA approach.

The predictive modeling initiated with the design of experiment (DoE) based on L_{27} OA of Taguchi method. The design parameters were orthogonally divided into low (L), medium (M) and high (H) level as clearly shown in Table 2. There were 27 individual experiments conducted according to the allocated level in each experimental rows and columns as shown in Table 3. The magnitudes of the output responses, FF and PCE for each experimental row were computed using (4) and (5) respectively as recorded in Table 4.

$$FF = \frac{V_{mp} J_{mp}}{V_{oc} J_{sc}} \quad (4)$$

$$PCE = \frac{J_{sc} \times FF \times V_{oc}}{P_{in}} \quad (5)$$

where V_{mp} and J_{mp} stand for voltage and current density at maximum power point respectively. Since FF and PCE were desired to be as large as possible, their respective magnitudes in each experimental row were required to be normalized based on larger-the-better objective problem formulated as:

$$x_i^*(k) = \frac{x_i(k) - \min x_i(k)}{\max x_i(k) - \min x_i(k)} \quad (6)$$

where $x_i^*(k)$, $x_i(k)$, $\min x_i(k)$ and $\max x_i(k)$ are the normalized data for each experimental row, the magnitude of output data for a certain experimental row, the minimum magnitude of the output data and the maximum magnitude of the output data respectively. The data normalization was then followed by computing the deviation sequences, $\Delta_{oi}(k)$ for every experimental row as:

$$\Delta_{oi}(k) = |x_o^*(k) - x_i^*(k)| \tag{7}$$

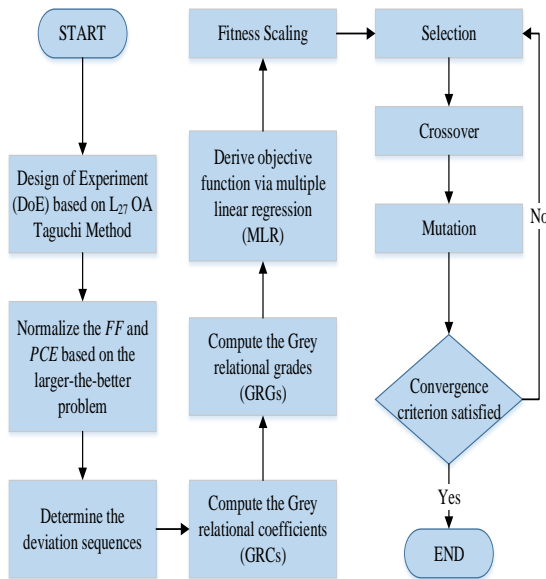


Figure 2 Flowchart of the predictive modeling using L_{27} OA Taguchi-based GRA-MLR-GA approach

Table 2 Levels of Design Parameters

Sym.	Parameter	Units	Level		
			Low (L)	Medium (M)	High (H)
A	SnO ₂ :F thickness	μm	0.2	0.4	0.6
B	SnO ₂ :F donor density	cm ⁻³	1×10 ¹⁸	5×10 ¹⁸	9×10 ¹⁸
C	ZnO thickness	μm	0.04	0.06	0.08
D	ZnO donor density	cm ⁻³	1×10 ¹⁷	5×10 ¹⁷	9×10 ¹⁷
E	CH ₃ NH ₃ PbI _{3-x} Cl _x thickness	μm	0.4	0.6	0.8
F	CH ₃ NH ₃ PbI _{3-x} Cl _x donor density	cm ⁻³	1×10 ¹³	5×10 ¹³	9×10 ¹³
G	Spiro-OMeTAD thickness	μm	0.25	0.35	0.45
H	Spiro-OMeTAD acceptor density	cm ⁻³	1×10 ¹⁸	5×10 ¹⁸	9×10 ¹⁸

Table 3 DoE based on L_{27} OA Taguchi

Exp . no.	A	B	C	D	E	F	G	H	FF (%)	PCE (%)
1	L	L	L	L	L	L	L	L	73.11	19.41
2	L	L	L	L	M	M	M	M	75.18	20.86
3	L	L	L	L	H	H	H	H	74.59	20.9
4	L	M	M	M	L	L	L	M	76.71	20.43
5	L	M	M	M	M	M	M	H	76.3	21.21
6	L	M	M	M	H	H	H	L	69.15	19.38
7	L	H	H	H	L	L	L	H	77.63	20.69
8	L	H	H	H	M	M	M	L	71.31	19.81
9	L	H	H	H	H	H	H	M	73.78	20.7
10	M	L	M	H	L	M	H	L	72.08	19.13
11	M	L	M	H	M	H	L	M	75.42	20.86
12	M	L	M	H	H	L	M	H	74.99	20.94
13	M	M	H	L	L	M	H	M	76.38	20.24
14	M	M	H	L	M	H	L	H	76.25	21.1
15	M	M	H	L	H	L	M	L	69.85	19.5
16	M	H	L	M	L	M	H	H	77.48	20.58
17	M	H	L	M	M	H	L	L	71.9	19.91
18	M	H	L	M	H	L	M	M	74.07	20.72
19	H	L	H	M	L	H	M	L	72.64	19.23
20	H	L	H	M	M	L	H	H	75.2	20.79
21	H	L	H	M	H	M	L	M	74.95	20.92
22	H	M	L	H	L	H	M	M	76.62	20.31
23	H	M	L	H	M	L	H	H	76.29	21.11
24	H	M	L	H	H	M	L	L	70.54	19.69
25	H	H	M	L	L	H	M	H	77.45	20.48
26	H	H	M	L	M	L	H	L	70.61	19.49
27	H	H	M	L	H	M	L	M	74	20.63

where $x_o^*(k)$ is the sequence referred to the unity which is normally set to 1. The deviation sequences for all the 27 experimental rows were then used in computing the grey relational coefficient (GRC), $\xi(k)$ formulated as:

$$\xi(k) = \frac{\Delta_{\min} + \xi\Delta_{\max}}{\Delta_{oi}(k) + \xi\Delta_{\max}} \tag{8}$$

where ξ is the distinguishing coefficient in the range of $0 \leq \xi \leq 1$. However, this particular study considered 0.5 as a magnitude of ξ because it offered moderate distinguishing effect and stability. Mathematically, any variation in the GRC would not contribute any changes in the overall rank of the grade. Based on Equation (8), the Δ_{\max} and Δ_{\min} are the maximum deviation magnitude and the minimum deviation magnitude respectively across the allocated columns. The average of the computed GRC for each experimental row were then measured based on the number of the involved output parameters. Since this case only involved two output parameters which were FF and PCE, the Grey relational grade (GRG), γ_i can be calculated as:

$$\gamma_i = \frac{1}{2} [\xi_1 + \xi_2] \tag{9}$$

Based on the interrelationship between eight input material parameters and the calculated GRGs, the objective function of the problem was derived via multiple linear regression (MLR) approach. Relationally, the MLR model for this particular study involving eight inputs and an output can be statistically expressed as:

$$Y = b_0 + b_1A + b_2B + b_3C + b_4D + b_5E + b_6F + b_7G + b_8H + e \quad (10)$$

where A, B, C, D, E, F, G and H are the investigated material parameters (SnO₂:F thickness, SnO₂:F donor density, ZnO thickness, ZnO donor density, CH₃NH₃PbI_{3-x}Cl_x thickness, CH₃NH₃PbI_{3-x}Cl_x donor density, Spiro-OMeTAD thickness and Spiro-OMeTAD acceptor density respectively), b_0 is the intercept, $b_1, b_2, b_3, b_4, b_5, b_6, b_7, b_8$ are the regression coefficients and e is the error term. For the estimation of the regression coefficients, the error terms will be neglected in which the objective function of the current problem can be simplified as:

$$Y' = b_0 + b_1A + b_2B + b_3C + b_4D + b_5E + b_6F + b_7G + b_8H \quad (11)$$

After identifying the objective function that summed up all the related problems, a well-known machine learning approach called Genetic Algorithm (GA) was employed to find the local optimal point of the objective function. The starting population for the problem is apparently the low level of the eight material parameters as tabulated in Table 3. The derived objective function was measurably scaled in the range of the pre-determined upper and lower boundaries so-called the fitness function (f_i). The Rastrigin function was utilized as a test function to evaluate the optimization algorithm due to multiple local minima type of problem which can be mathematically expressed as:

$$Ras(x) = 10n + \sum_{i=1}^n [x_i^2 - 10 \cos(2\pi x_i)] \quad (12)$$

where n is a total number of the input material parameters and x_i is the output parameter (GRG). The Rastrigin function is appraised based on the hypercube $x_i \in [-5.12, 5.12]$ for all $i = 1, 2, 3, 4, 5, 6, 7$ and 8 . Since this function was originally designed for finding the local minima of the curve, it was instead inverted to find the local maxima of the objective curve. Hence, the fitness function (f_i) for this case study (larger-the-better problem) can be mathematically formulated as listed in Table 4.

After repeating the process of selection, crossover and mutation, the best magnitude of the fitness function would be eventually identified. For adequate number of generations, those processes were iterated until no significant improvement detected in the fitness magnitude. At this point, the best magnitude of

the fitness function was regarded as the new emerging populations of parameter A (SnO₂:F thickness), parameter B (SnO₂:F donor density), parameter C (ZnO thickness), parameter D (ZnO donor density), parameter E (CH₃NH₃PbI_{3-x}Cl_x thickness), parameter F (CH₃NH₃PbI_{3-x}Cl_x donor density), parameter G (Spiro-OMeTAD thickness) and parameter H (Spiro-OMeTAD acceptor density) were able to be optimally forecasted. The default GA preferences for this case study were set as:

Type = real-valued
Population size = 50
Number of generations = 1000
Elitism = 2
Crossover probability = 0.8
Mutation probability = 0.1

Table 4 Fitness function (f_i) formulation for larger-the-better problem

Minimize - Ras(A, B, C, D, E, F, G, H)	
Subject to the constraints:	
A	$0.18 \mu\text{m} \leq A \leq 0.62 \mu\text{m}$
B	$1 \times 10^{18} \text{ cm}^{-3} \leq B \leq 9 \times 10^{18} \text{ cm}^{-3}$
C	$0.038 \mu\text{m} \leq C \leq 0.082 \mu\text{m}$
D	$1 \times 10^{17} \text{ cm}^{-3} \leq D \leq 9 \times 10^{17} \text{ cm}^{-3}$
E	$0.38 \mu\text{m} \leq E \leq 0.82 \mu\text{m}$
F	$1 \times 10^{13} \text{ cm}^{-3} \leq F \leq 1 \times 10^{13} \text{ cm}^{-3}$
G	$0.23 \mu\text{m} \leq G \leq 0.47 \mu\text{m}$
H	$1 \times 10^{18} \text{ cm}^{-3} \leq H \leq 9 \times 10^{18} \text{ cm}^{-3}$

3.0 RESULTS AND DISCUSSION

Before undergoing further on predictive modeling approach, a simple experiment has been done to observe the effect of parameter variations on the device performances. Table 5 shows the summary of the effects of single parameter variations on their corresponding PCE. (Note: Default parameters are set similarly to medium level as indicated in Table 2.)

Based on Table 5, material parameters; SnO₂:F donor density, ZnO donor density, CH₃NH₃PbI_{3-x}Cl_x donor density, Spiro-OMeTAD thickness and Spiro-OMeTAD acceptor density indicate a very least influence on the PCE variation as there is no changes in PCE detected. Material parameters; SnO₂:F thickness and ZnO thickness exhibit increasing trend in PCE as their corresponding thickness are reduced. On the other hand, material parameter; CH₃NH₃PbI_{3-x}Cl_x thickness demonstrates declining trend in PCE as its thickness is reduced.

The collective results of the predictive modeling of the Perovskite photovoltaic cell are presented in this section. The experimental data resulted from the DoE L₂₇ Taguchi OA in Table 3 are normalized accordingly where the deviation sequences, the GRCs, GRGs and their respective ranks for each experimental row are computed, evaluated and recorded in Table 6.

Table 5 Summary of the effects of parameter variations on their corresponding PCE

SnO ₂ :F thickness (μm)	PCE (%)	Trend	SnO ₂ :F donor density (cm ⁻³)	PCE (%)	Trend
0.2	20.04	↑	1×10 ¹⁸	19.98	No changes
0.4	19.98		5×10 ¹⁸	19.98	
0.6	19.93		9×10 ¹⁸	19.98	
ZnO thickness (μm)	PCE (%)	Trend	ZnO donor density (cm ⁻³)	PCE (%)	Trend
0.04	19.98	↑	1×10 ¹⁷	19.98	No changes
0.06	19.98		5×10 ¹⁷	19.98	
0.08	19.97		9×10 ¹⁷	19.98	
CH ₃ NH ₃ PbI _{3-x} Cl _x thickness (μm)	PCE (%)	Trend	CH ₃ NH ₃ PbI _{3-x} Cl _x donor density (cm ⁻³)	PCE (%)	Trend
0.4	18.79	↓	1×10 ¹³	19.98	No changes
0.6	19.98		5×10 ¹³	19.98	
0.8	20.45		9×10 ¹³	19.98	
Spiro-OMeTAD thickness (μm)	PCE (%)	Trend	Spiro-OMeTAD acceptor density (cm ⁻³)	PCE (%)	Trend
0.25	19.98	No changes	1×10 ¹⁸	19.98	No changes
0.35	19.98		5×10 ¹⁸	19.98	
0.45	19.98		9×10 ¹⁸	19.98	

Table 6 Deviation Sequences, GRCs, GRGs and Ranks

Exp. No.	Deviation Sequences, Δ _{oi} (k)		GRC, ξ _i (k)		GRG (y _i)	Rank
	Δ _{oi} (FF)	Δ _{oi} (PCE)	ξ _i (FF)	ξ _i (PCE)		
	1	0.5330	0.8654	0.4840		
2	0.2889	0.1683	0.6338	0.7482	0.6910	11
3	0.3585	0.1490	0.5824	0.7704	0.6764	12
4	0.1085	0.375	0.8217	0.5714	0.6966	10
5	0.1568	0	0.7612	1	0.8806	1
6	1	0.8798	0.3333	0.3624	0.3479	27
7	0	0.25	1	0.6667	0.8333	3
8	0.7453	0.6731	0.4015	0.4262	0.4139	21
9	0.4540	0.2452	0.5241	0.6710	0.5975	17
10	0.6545	1	0.4331	0.3333	0.3832	24
11	0.2606	0.1683	0.6574	0.7482	0.7028	8
12	0.3113	0.1298	0.6163	0.7939	0.7051	7
13	0.1474	0.4663	0.7723	0.5174	0.6449	15
14	0.1627	0.0529	0.7544	0.9044	0.8294	4
15	0.9175	0.8221	0.3527	0.3782	0.3655	26
16	0.0177	0.3029	0.9658	0.6228	0.7943	5
17	0.6757	0.625	0.4253	0.4444	0.4349	19
18	0.4198	0.2356	0.5436	0.6797	0.6117	16
19	0.5884	0.9519	0.4594	0.3444	0.4019	22
20	0.2866	0.2019	0.6357	0.7123	0.6740	13
21	0.3160	0.1394	0.6127	0.7820	0.6973	9
22	0.1191	0.4327	0.8076	0.5361	0.6719	14
23	0.1580	0.0481	0.7599	0.9123	0.8361	2
24	0.8361	0.7308	0.3742	0.4063	0.3902	23
25	0.0212	0.3510	0.9593	0.5876	0.7734	6
26	0.8278	0.8269	0.3766	0.3768	0.3767	25
27	0.4281	0.2788	0.5388	0.6420	0.5904	18

The experimental results from the GRA in Table 6 reveals that the highest rank of GRG demonstrated by the fifth experimental row, indicating that the fifth row contains the best levels of the input material parameters which would possibly generate the most optimum magnitude of FF and PCE of the device. Figure 3 shows the interrelationship between eight input material parameters and the computed GRGs developed using MLR approach. The scattered points on the plot are observed to form a curve rather than

a straight line implying the skewness in the computed GRGs. In this case, most of GRG points are scattered near the reference line, implying that the GRGs are reasonably consistent with normality.

The summary of the MLR results for this case study is tabulated in Table 7. From the results, the input material parameter that dominantly contribute the most impact on the GRG variations is parameter H (Spiro-OMeTAD acceptor density) with three significant code, followed by parameter E (CH₃NH₃PbI_{3-x}Cl_x thickness) with one significant code. The remaining of the involved material parameters are considered neutral as their respective magnitudes would not contribute significant impact on the GRG variations.

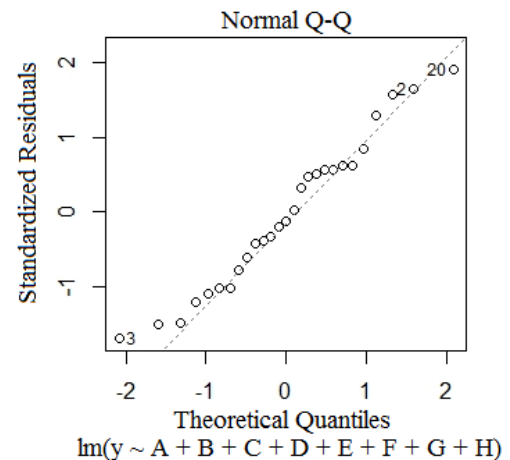


Figure 3 Q-Q plots for multiple input parameters

The objective function of the current problem can be drawn from the computed estimation of regression coefficients and relationally written as:

$$Y' = 0.545 - 0.042A + 0.001B - 0.205C + 0.002D - 0.178E - 0.001F - 0.149G + 0.048H \tag{13}$$

The objective function is required to be inverted within the pre-determined upper and lower boundaries due to the equation is originally derived for searching the local minima.

Table 7 Summary of Multiple Linear Regressions

Term	Regression Coeff.	Std. Error	t value	Pr (> t)	Signif. code
Intercept	0.5454974	0.0870634	6.266	6.57e-06	***
A	-0.0417837	0.0678473	-0.616	0.546	
B	0.0009617	0.0033924	0.283	0.780	
C	-0.2049723	0.6784730	-0.302	0.766	
D	0.0022402	0.0033924	0.660	0.517	
E	-0.1784969	0.0678473	-2.631	0.017	*
F	-0.0012224	0.0033924	-0.360	0.723	
G	-0.1494892	0.1356946	-1.102	0.285	
H	0.0484275	0.0033924	14.275	2.94e-11	***

Significant Code: 0 '***', 0.001 '**', 0.01 '*', 0.05 '.' 0.1 '-'

Hence, the fitness function of the maximization problem can be mathematically re-written as:

$$Y' = -0.545 + 0.042A - 0.001B - 0.205C - 0.002D + 0.178E + 0.001F + 0.149G - 0.048H \quad (14)$$

The fitness function (*f_i*) iteratively undergoes the process of selection, crossover and mutation until the optimum magnitude of the function is reached. For this case, the process of selection, crossover and mutation were halted at 941 iterations as illustrated in Figure 4.

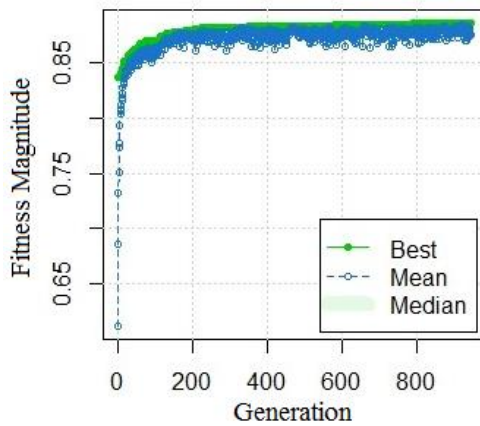


Figure 4 GA Performance during convergence

Based on the GA performance, the highest possible fitness magnitude of the GRG is observed at 0.886558 where the optimum magnitude of the input material parameters; A, B, C, D, E, F, G and H are predictively estimated at 0.198 μm, 8.973x10¹⁸ cm⁻³, 0.039 μm, 8.827x10¹⁷ cm⁻³, 0.386 μm, 1.929x10¹³ cm⁻³, 0.233 μm and 8.984x10¹⁸ cm⁻³ respectively.

Finally, the Perovskite photovoltaic cell model is re-simulated by employing the newly predicted input material parameters for verification. The comparative J-V transfer characteristics of the device between before and after predictive modeling are depicted in Figure 5.

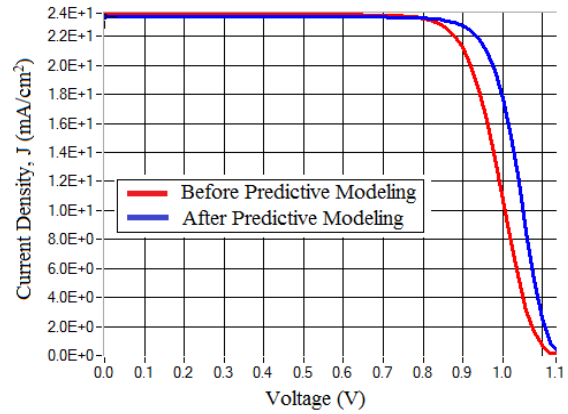


Figure 5 J-V transfer characteristics of Perovskite photovoltaic cell before and after predictive modelling

Based on the J-V curves, the open circuit voltage (*V_{oc}*) of the device has been slightly enhanced by ~0.51% after undergoing the proposed predictive modeling approach where the *V_{oc}* magnitude before and after predictive modeling are measured at 1.1282 V and 1.1340 V respectively. However, a slight decrease of ~0.7% in current density (*J_{sc}*) demonstrated by the device after predictive modeling predominantly attributed to larger resistive losses that sourced from erratic variation effect of thickness and dopant density in absorber layer. *J_{sc}* magnitudes for both devices before and after predictive modeling are measured at 23.535 mA/cm² and 23.371 mA/cm² respectively. Figure 6 depicts the comparative bar graph of FF and PCE before and after predictive modeling. According to the bar graph, a slight rise exhibited in both output parameters after undergoing the proposed predictive modeling approach (Hybrid L₂₇ OA Taguchi-based GRA-MLR-GA) in which both FF and PCE are improved by ~5.93% and ~5.78% respectively.

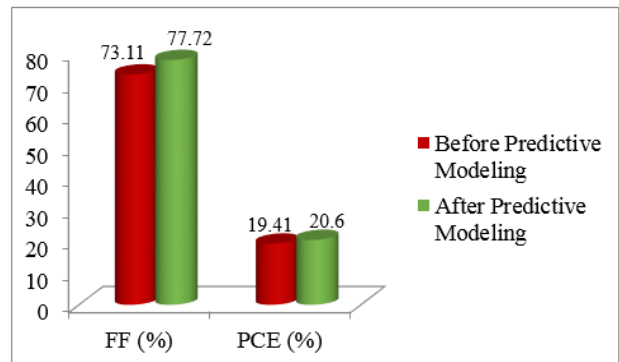


Figure 6 Comparative bar graph of FF and PCE before and after predictive modeling

Table 8 summarizes the improvement of *FF* and *PCE* after the input material parameters have been predictively modeled by the proposed approach. The experimental results explicitly prove that the electrical performance of Perovskite photovoltaic cell can be significantly improved by predictively modeling the input material parameters using the proposed hybrid L_{27} OA Taguchi-based GRA-MLR-GA approach. In future work, more input material parameters could be added into the existing analytical model in order to gain better predictive solutions.

Table 8 Summary of Device Modeling Using Hybrid L_{27} OA Taguchi-based GRA-MLR-GA Approach

Output Parameters	Units	Before Predictive Modeling	After Predictive Modeling	% Improvement
<i>FF</i>	%	73.11	77.72	~5.93%
<i>PCE</i>	%	19.41	20.6	~5.78%

4.0 CONCLUSION

In summary, the Perovskite photovoltaic cell virtually developed via open source solar cell capacitance simulator (SCAPS) has been successfully optimized using the proposed hybrid L_{27} OA Taguchi-based GRA-MLR-GA approach. The proposed approach utilized L_{27} OA Taguchi design of experiments (DoE) for experimental data acquisition. The Grey relational analysis (GRA) was subsequently conducted to merge two types of experimental data (*FF* & *PCE*) into a single representative unit called Grey relational grade (GRG). Through multiple linear regression (MLR) analysis, the objective function of the centered problem was drawn and fed into genetic algorithm for searching local maxima of the function. After iteratively undergoing 941 cycles of selection, crossover and mutation, the best fitness magnitude (f_i) was found at 0.886558. The optimum magnitude of the material parameters have been successfully obtained as shown in Table 9.

Table 9 Optimum Magnitude of the Material Parameters

Material Parameters	Optimum Magnitude
SnO ₂ :F thickness	0.198 μm
SnO ₂ :F donor density	$8.973 \times 10^{18} \text{ cm}^{-3}$
ZnO thickness	0.039 μm
ZnO donor density	$8.827 \times 10^{17} \text{ cm}^{-3}$
CH ₃ NH ₃ PbI _{3-x} Cl _x thickness	0.386 μm
CH ₃ NH ₃ PbI _{3-x} Cl _x donor density	$1.929 \times 10^{13} \text{ cm}^{-3}$
Spiro-OMeTAD thickness	0.233 μm
Spiro-OMeTAD acceptor density	$8.984 \times 10^{18} \text{ cm}^{-3}$

Furthermore, both *FF* and *PCE* of the device were successfully improved by ~5.93% and ~5.78% respectively. These explicitly justify that the proposed hybrid L_{27} OA Taguchi-based GRA-MLR-GA approach could be suitably employed in modeling multiple material parameters of Perovskite photovoltaic cell for improved performance.

Acknowledgement

The authors would like to thank the Ministry of Higher Education (MOHE) of Malaysia, Mybrain15 and Micro and Nano Electronics Research Group (MiNE), Centre for Telecommunication Research and Innovation (CeTRI), Faculty of Electronics and Computer Engineering (FKEKK), Universiti Teknikal Malaysia Melaka (UTeM) for sponsoring this research study under research grant (FRGS/1/2017/TK04/FKEKK-CeTRI/F00335).

References

- [1] Sun, Y., Seo, J. H., Takacs, C. J., Seifert, J., and Heeger, A. J. 2011. Inverted Polymer Solar Cells Integrated with a Low-Temperature-Annealed Sol-Gel-Derived ZnO Film as an Electron Transport Layer. *Advanced Materials*. 23(14): 1679-83.
- [2] Tara, A., Bharti, V., Sharma, S., and Gupta, R. 2021. Device Simulation of FASnI₃ based Perovskite Solar Cell with Zn(O_{0.3}, S_{0.7}) as Electron Transport Layer using SCAPS-1D. *Optical Materials*. 119: 111362.
- [3] Hussain, S. S., Riaz, S., Nowsherwan, G. A., Jahangir, K., Raza, A., Iqbal, M. J., Sadiq, I., Hussain, S. M., and Naseem, S. 2021. Numerical Modeling and Optimization of Lead-Free Hybrid Double Perovskite Solar Cell by Using SCAPS-1D. *Journal of Renewable Energy*. 2021: 1-12.
- [4] Yongjin, G., Xueguang, B., Yucheng, L., Binyi, Q., Qingliu, L., Qubo, J., and Pei, M. 2020. Numerical Investigation Energy Conversion Performance of Tin-based Perovskite Solar Cells Using Cell Capacitance Simulator. *Energies*. 13(5907): 1-17.
- [5] Noh, J. H., Im, S. H., Heo, J. H., Mandal, T. N., and Il Seok, S. 2013. Chemical Management for Colorful, Efficient, and Stable Inorganic-Organic Hybrid Nanostructured Solar Cells. *Nano Letters*. 13: 1764-1769.
- [6] Kumawat, N. K., Dey, A., Kumar, A., Gopinathan, S. P., Narasimhan, K. L., and Kabra, D. 2015. Band Gap Tuning of CH₃NH₃Pb(Br_{1-x}Cl_x)₃ Hybrid Perovskite for Blue Electroluminescence. *ACS Applied Materials and Interfaces*. 7(24): 13119-24.
- [7] Lin, L., Jiang, L., Li, P., Fan, B., and Qiu, Y. 2018. A Modeled Perovskite Solar Cell Structure with a Cu₂O Hole-transporting Layer Enabling over 20% Efficiency by Low-cost Low-temperature Processing. *Journal of Physics and Chemistry of Solids*. 124(July 2018): 205-11.
- [8] Haider, S. Z., Anwar, H., and Wang, M. 2018. A Comprehensive Device Modelling of Perovskite Solar Cell with Inorganic Copper Iodide as Hole Transport Material. *Semiconductor Science and Technology*. 33(3): 1-12.
- [9] Mandadapu, U., Vedanayakam, S. V., Thyagarajan, K., and Babu, B. J. 2018. Optimisation of High Efficiency Tin Halide Perovskite Solar Cells using SCAPS-1D. *International Journal of Simulation and Process Modelling*. 13 (3): 221-27.
- [10] Bello, I. T., Odedunmoye, Y. A., Adedokun, O., Shiitu, H. A., and Audugba, A. O. 2019. Numerical Simulation of Sandwiched Perovskite-based Solar Cell Using Solar Cell Capacitance Simulator (SCAPS-1D). *Journal of the Nigerian Society of Physical Sciences*. 1(2019): 57-61.
- [11] Du, H. J., Wang, W. C., and Gu, Y. F. 2017. Simulation Design of P-I-N-type all-perovskite Solar Cells with High Efficiency. *Chinese Physics B*. 26 (2): 1-7.
- [12] Mandadapu, U., Vedanayakam, S. V., Thyagarajan, K., Reddy, M. R., and Babu, B. J. 2017. Design and Simulation of High Efficiency Tin Halide Perovskite Solar Cell. *International Journal of Renewable Energy Research*. 7(4): 1604-12.
- [13] Kaharudin, K. E., Salehuddin, F., Hamidon, A. H., Aziz, M. N. I. A. and Ahmad, I. 2015. Taguchi Modeling of Process

- Parameters in VDG-MOSFET Device for Higher I_{ON}/I_{OFF} Ratio. *Jurnal Teknologi*. 77(12): 19-26.
- [14] Salehuddin, F., Kaharudin, K. E., Zain, A. S. M., Yamin, A. K. M., and Ahmad, I. 2014. Analysis of Process Parameter Effect on DIBL in n-channel MOSFET Device using L_{27} Orthogonal Array. *International Conferences on Fundamental and Applied Sciences. AIP Conf. Proc.* 1621 (1): 322-28.
- [15] Roslan, A. F., Kaharudin, K. E., Salehuddin, F., Zain, A. S. M., Ahmad, I., Faizah, Z. A. N., Hazura, et al. 2018. Optimization of 10 nm Bi-GFET Device for Higher I_{ON}/I_{OFF} Ratio Using Taguchi Method. *Journal of Physics: Conference Series*. 1123: 012046.
- [16] Kaharudin, K. E., Salehuddin, F., Zain, A. S. M., and Roslan, A. F., 2019. Optimal Design of Junctionless Double Gate Vertical MOSFET using Hybrid Taguchi-GRA with ANN Prediction. *Journal of Mechanical Engineering and Sciences*. 13(3): 5455-79.
- [17] Kaharudin, K. E., Hamidon, A. H., Salehuddin, F. 2014. Implementation of Taguchi Modeling for Higher Drive Current (I_{ON}) in Vertical DG-MOSFET Device. *Journal of Telecommunication, Electronic and Computer Engineering*. 6(2): 11-18.
- [18] Kaharudin, K. E., Salehuddin, F., Zain, A. S. M., and Aziz, M. N. I. A. Taguchi Modeling with the Interaction Test for Higher Drive Current in WSi_x/TiO_2 Channel Vertical Double Gate NMOS Device. *Journal of Theoretical and Applied Information Technology*. 90(1): 185-93.
- [19] Niemegeers, A., Burgelman, M. 1996. Modelling of AC-Characteristics of Solar Cells. *Proc. 25nd IEEE Photovoltaic Specialists Conference*. 901-4.
- [20] Hossain, M. F., Faisal, M., and Okada, H. 2016. Device Modeling & Performance Analysis of Perovskite Solar Cells based on Similarity with Inorganic Thin Film Solar Cells Structure. *International Conference on Electrical, Computer and Telecommunication Engineering*. 8-10.
- [21] Sobayel, K., Akhtaruzzaman, M., Rahman, K. S., Ferdaous, M. T., Al-Mutairi, Z. A., Alharbi, H. F., Alharthi, N. H. Karim, M. R., Hasmady, S., and Amin, N. 2019. A Comprehensive Defect Study of Tungsten Disulfide (WS_2) as Electron Transport Layer in Perovskite Solar Cells by Numerical Simulation. *Results in Physics*. 12(December 2018): 1097-1103.